Published in final edited form as:
Nature. 2010 July 8; 466(7303): 203–208. doi:10.1038/nature09153.

Structural mechanism of C-type inactivation in K+ channels

Luis G. Cuello[*,1], **Vishwanath Jogini**[*,2], **D. Marien Cortes**[1], and **Eduardo Perozo**
Department of Biochemistry and Molecular Biology, and Institute for Biophysical Dynamics, University of Chicago, IL-60637

Abstract

Interconversion between conductive and non-conductive forms of the K^+ channel selectivity filter underlies a variety of gating events, from flicker transitions (μs) to C-type inactivation (ms-s). Here, we report the crystal structure of the K^+ channel KcsA in its Open-Inactivated conformation and investigate the mechanism of C-type inactivation gating at the selectivity filter from channels "trapped" in a series of partially open conformations. Five conformer classes were identified with openings ranging, from 12 Å in closed KcsA (Cα-Cα distances at T112) to 32 Å when fully open. They revealed a remarkable correlation between the degree of gate opening and the conformation and ion occupancy of the selectivity filter. We show that a gradual filter backbone reorientation leads first, to a loss of the S2 ion binding site and a subsequent loss of the S3 binding site, presumably abrogating ion conduction. These structures suggest a molecular basis for C-type inactivation in K^+ channels.

The functional behaviour of most ion channels is defined by the relationship between two coupled mechanisms: activation and inactivation gating. Activation is associated with a large hinged motion around the inner helix bundle, as observed in a number of K^+ channel structures[1,2,3,4,3,4,5,6], and characterized spectroscopically in KcsA[7,8,9,10,11]. Inactivation typically takes place in a stimulus independent way, though it is sometimes coupled to the activation process[12,13]. In K^+ channels, inactivation gating can occur by two distinct molecular mechanisms: N-type inactivation, a fast, autoinhibitory process where an N-terminal particle binds to the open pore, blocking conduction[14]; and C-type inactivation, which originates from transitions at the selectivity filter[15,16]. C-type inactivation often (though not always) develops with much slower kinetics and is highly modulated by permeant ions and pore blockers[17,18,19,20,21].

Coordination of K^+ ions at the selectivity filter establishes unique structural constraints in order to optimally select against impermeable ions while allowing for fast K^+ ion translocation[22,23,24]. Therefore, perturbations in selectivity filter geometry can have

Correspondence to: Eduardo Perozo, eperozo@uchicago.edu, Ph: (773) 834-4747.
*These authors contributed equally to this work
[1]Department of Cell Physiology and Molecular Biophysics, Texas Tech University Lubbock, TX, USA.
[2]D. E. Shaw Research, Hyderabad, India

Supplementary Information is linked to the online version of the paper at www.nature.com/nature.

Author Contributions

E.P. and L.G.C. conceived the project. L.G.C and D.M.C generated constructs, performed biochemical analysis, expressed, purified and crystallized the proteins. L.G.C. performed electrophysiology experiments. L.G.C, V.J. and E.P collected X-ray diffraction data. L.G.C and V.J. determined and analyzed the structures. E.P., L.G.C and V.J. analyzed the data and wrote the paper.

Author Information

The atomic coordinates and structure factors of OM-KcsA in the Open-Inactivated conformation and four additional partially open structural classes have been deposited with the Protein Data bank under the following accession numbers: Open 32 Å, 3F5W; Open 23 Å, 3F7V; Open 17 Å, 3F7Y; Open 15 Å, 3FB6; and Open 14 Å, 3BF5. Reprints and permissions information is available at www.nature.com/reprints.

significant consequences on its ability to conduct ions, making the filter an energetically economic gate. Indeed, a number of independent pieces of evidence point to the selectivity filter as a region with a great deal of influence over the gating behaviour of a channel, including long-lasting C-type inactivation[16,18,25,26,27,28], as well as the fast gating events observed in most single channel recordings ("Flicker" transitions). Furthermore, under saturating conditions, gating transitions are dominated by conformational fluctuations at the selectivity filter[25,29,30,31].

Here, we report a series of crystal structures of KcsA transitioning between a conformation where the inner gate is closed and the selectivity filter is conductive (Closed-Conductive) to one in which the inner gate is fully open and the selectivity filter is inactivated (Open-Inactivated). By solving multiple structures of a constitutively open KcsA mutant[32], we show that the conformation of the selectivity filter in its inactivated state is reminiscent of that of a filter under low ionic conditions[33,34], but at high K^+ concentrations. This set of partially open KcsA structures provides a thorough description of the inactivated filter and helps establish the likely conformational transitions between the conductive and C-type inactivated forms of the selectivity filter. In an accompanying manuscript, we propose a mechanism for the bi-directional coupling between the activation and inactivation gates, with implications to the more complex eukaryotic K^+ channels [35].

Crystal structure of Open-Inactivated KcsA

In KcsA, a cluster of charged residues located at the intracellular end of TM1 and TM2 was identified as the putative proton sensor[36,37]. Engineering an excess of negative charge by neutralizing all but one of the members of this charge cluster (E118) leads to a constitutively open mutant channel (KcsA-OM)[32], as suggested by in-vivo, radiotracer flux assays and single channel measurements (Supplementary material, Fig S1).

Early attempts at crystallizing a C-terminal truncated form of KcsA-OM (H25Q, R117Q, E120Q, R121Q, R122Q and H124Q) in complex with an antibody fragment (tKcsA-OM/Fab) yielded well-behaved diffracting crystals, but revealed only marginally open channels[32]. We reasoned that since the complex in the crystal lattice is arranged so that the Fab clasps the lower gate of a neighbouring complex, lattice forces were responsible for closing the channel. To create enough space for TM2 movement, we truncated the N-terminal helix (tKcsA-OM Δ1-20), crystallized the shortened construct and solved its structure by molecular replacement with refinement statistics, R_{work}/R_{free} of 25.9/27.6 (Supplementary material, Table I). The resulting 3.2 Å resolution tKcsA-OM Δ1-20 structure (Fig. 1a) has a fully open gate generating a large, water-filled cavity on the intracellular face of the channel as a consequence of the hinge-bending motion and rotation of TM2 (Supplementary material Fig S2). But the key feature of this structure is that the conformation of the selectivity filter is significantly different from that seen in the closed state[34] (Fig. 1b).

We suggest that this structure represents the Open-Inactivated conformation of the channel and is characterized by ion vacancies at positions S2 and S3 of the selectivity filer, with ions occupying only S1 and S4 (Fig. 1b). The filter itself shows a ~ 2 Å narrowing of the conduction pathway due to the movement of G77 (Fig. 1c). Although the actual location of the carbonyls groups cannot be precisely established at the present resolution, our best-fitted models closely resemble the structure of the KcsA filter in low K^+ [34], even though all our crystals were obtained at high K^+ concentrations. This similarity strongly suggests that the structure of the selectivity filter in the Close-Inactivated state[38] is best represented by the low K^+ filter structure[34], as previously suspected[39,40,41]. There are, however, some subtle differences between the low K^+ filter and a C-type inactivated one. First, unlike the low K^+

structure we find no significant electron density in the S3 binding site[34]. Second, the lower part of the filter expands ~1.5 Å, increasing the accessible area in S3–S4 binding sites. Finally, there is a slight change in pitch of the pore helix in the first turn and a half from the inner cavity (Supplementary material Figure. S3).

A wealth of functional data suggests that in eukaryotic K^+ channels C-type inactivation involves a localized constriction in the outer vestibule of the selectivity filter[42,26,43]. However, even after considering the pore constriction near G77, the present Open-Inactivated structure shows only subtle rearrangements in the external vestibule when compared to the Close-Conductive structure (Fig. 1c). We suggest that while its average conformation remains essentially unchanged, the filter might be capable of backbone and side chain sojourns that transiently place outer vestibule residues within crosslinking range (4–5 Å)[42].

Additional functional and structural data point to the critical role that the network of hydrogen bonds immediately behind the selectivity filter plays in C-type inactivation. We have shown that in KcsA, the rate and extent of C-type inactivation is governed by interactions involving residues W67, E71 and D80 behind the selectivity filter[25,44]. It has been proposed that the strength of these interactions is proportional to the rate and extent of C-type inactivation, which could promote a subtle compression between the pore helix and the external vestibule[44]. This suggestion is compatible with the change in helical pitch at the base of the pore helix. Interestingly, the side chain of E71, a residue that deeply influences C-type inactivation in KcsA, seems to undergo a large rotameric reorientation of about 90 degrees which could potentially modify the strength of the carboxyl-carboxylate interaction with residue D80[34].

Open KcsA in multiple conformations

While screening for high quality crystals, we noticed significant variability in the conformation of TM2 after initial electron densities were obtained and refined for 25 tKcsA-OM Δ1-20 crystals. Non-redundant structures were analyzed (Fig 2) by computing two diagnostic parameters: the angle (Ψ) between the C-terminal half of TM2 (below the G104 hinge) and the z-axis of the channel (from the position of the ions in the filter), and the angle (φ) between the two sections of TM2 (flanking the G104 hinge). From these measurements, we identified four major structural classes of partial and full openings, which we have named according to the average diameter for the inner helix opening, empirically defined as the Cα-Cα distances at position T112. These are, Open 15 Å, Open 17 Å, Open 23 Å and Open 32 Å (the equivalent distance in the closed conformation is ~12 Å). The top panels in Fig. 2 are representative composite omit maps for each structural class (More detailed maps of the selectivity filter are shown in Supplementary material Fig S4). The rather heterogeneous 15 Å open class spans openings between 14–16 Å.

All of the structures were obtained as Fab-Channel complexes using identical conditions[32]. At this time, it is difficult to quantitatively explain the origin of this fortuitous outcome, though it is possible that PEG-driven crystal dehydration might have played a role. However, if we assume that in the crystal lattice TM2 hinge-bending transitions between partially and fully open states transit a fairly shallow energy landscape, it is possible that minute variations in initial conditions and crystal nucleation would lead to the stabilization of distinct partial openings. In support of this, we found a correlation between the degree of opening and the nominal resolution of each individual dataset, in which larger diameter openings are always associated with lower resolutions (Supplementary material Fig S5).

Sequential changes at the selectivity filter

Although resolution issues limit our interpretation of the detailed changes in the selectivity filter, two lines of evidence suggest that the structural classes we have identified can be understood in terms of a putative sequence of conformational transitions leading to the C-type inactivated filter. First, the sequential increase in the diameter of the inner cavity, from the closed state to the Open 32 Å class (Supplementary material Fig S6), logically lends itself to be interpreted as a "chronology" of gating. Second, consideration of the subtler changes at the selectivity filter associated to each structural class argues strongly for step-wise transitions connecting the conductive to the non-conductive filter (Supplementary material Fig S7). Indeed, the extent and magnitude of the conformational change in the filter is local and rather limited until the transition between Open 17 and Open 23, which we suggest is the main conformational transition defining the C-type inactivated conformation.

This correlation is shown in Figure 3 and Supplementary material Figure S8, where the diagonally related inter-subunit Cα-Cα distance at Gly77, decreases as a function of the inner bundle diameter (Cα-Cα distances at Thr112). Transitions from the nominally closed state to two limited opening structures (in the Open 15 Å class) generate a slight increase in distance, followed by a further narrowing in the Open 17 Å structure. The main structural transition involves a ~2 Å pinching which ultimately leads to the non-conductive form of the filter observed both in the Open 23 Å and Open 32 Å classes.

Correlation between gate opening and ion occupancy at the selectivity filter

Just as in the distribution of inner gate conformations (Fig 2), close observation of the selectivity filter electron density maps from all analyzed structures revealed additional structural heterogeneity among the Open 15 Å class in terms of ion occupancy. Although similar in filter backbone conformation, some structures showed the full aggregate occupancy of four ions, whereas a few structures were characterized by a significant loss of density in site S2. Figure 4a shows representative examples of composite omit maps of the selectivity filter (blue mesh) and $F_o - F_c$ omit map (ions, magenta mesh), for two different members of the Open 15 Å class (open at 14 and 16 Å), in addition to the 17, 23 and 32 Å classes. A more quantitative estimate of the correlation between filter occupancy and inner bundle gate opening can be obtained from one-dimensional electron density maps[23]. However, while the present electron density differences are mechanistically significant, determination of actual occupancies requires the use of an anomalous signal (i.e. Tl^+). Therefore, these estimates should be considered only in terms of relative occupancies.

The z axis density profiles from all structural classes (Figure 4b) show the positions of the individual ion binding sites. At the narrowest opening (14 Å) we find four evenly distributed peaks of similar area (though S2 is already slightly smaller), reminiscent of the occupancy of the conductive filter conformation. As the inner bundle gate opens further, the profile changes considerably. Ion occupancy at S2 is reduced at 15 Å opening and is completely eliminated at 17 Å. The peak at S3, on the other hand is more resilient, showing strong density up to openings of 17 Å, to disappear abruptly after the key transition from 17 to 23 Å opening. The peaks corresponding to S1 and S4 remain strong for all gate openings; however, as the filter undergoes structural rearrangements leading to its fully C-type inactivated conformation, there is a clear contraction in the position of the ions which narrow some 4 Å between the 17 and 23 Å openings.

The picture that emerges suggests that at the onset of C-type inactivation, the sequence of backbone rearrangements has an early influence on the ability of the S2 site to coordinate ions. S3 is only affected after the gate opens significantly (23 Å), probably as a direct consequence of the narrowing of the filter by the movement of Gly77. This is shown in Fig

4c where the relative areas derived from Gaussian fits to the whole electron density profile are plotted as a function of the inner bundle diameter (Cα-Cα distances at Thr112). Computational analyses have suggested that S2 is the most K^+ selective site in the selectivity filter[45], an observation that might help explain the known loss of K^+ selectivity (and increased Na^+ permeability) by most K^+ channels during C-type inactivation[17,18].

Can we establish which of these conformations (if any) is able to support ion conduction and at which point is conduction fully abrogated? We propose that the K^+ selectivity filter is unable to conduct ions only when two sequential ion binding sites (S2 and S3) are compromised by rearrangements in the backbone conformation at or near Gly77 (Fig 3). But like Rb^+, with an aggregate occupancy of three ions in the filter[23,33], a K^+ ion going through the selectivity filter is likely to overcome a single unstable binding site. Consequently, we argue that of all the structural classes presently under consideration, only the Open 23 Å and Open 32 Å classes are non-conductive at the level of the selectivity filter.

A molecular mechanism of C-type inactivation

The different structural classes observed for the constitutively open mutant of KcsA point to a mechanism of inactivation with a specific sequence of structural transitions. We must point out, however, that these partially open/inactivated structures cannot be considered as strict kinetic intermediaries in the context of the K^+ channel gating cycle. In a simple four-state scheme that includes a Closed-Conductive (C/O), an Open-Conductive (O/O), an Open-Inactivated (OI) and a Closed-Inactivated (CI) state:

$$\begin{array}{ccc} (C/O) & \leftrightarrow & (O/O) \\ \updownarrow & & \updownarrow \\ (C/I) & \leftrightarrow & (O/I) \end{array}$$

C-type inactivation develops once the channel reaches the Open-Conductive conformation (O/O), a pathway which presumes complete gate opening. Thus, it would be expected that partially inactivated filters ought to be mostly associated with channels displaying a fully open inner gate. Instead, the present structures are a mixture of partially open inner gates and partial C-type inactivated filters, in a way that would suggest a diagonal pathway between C/O and O/I (Fig 5a). Although these results are consistent with recent experimental evidence showing that C-type inactivation can develop from partially open channels showing little or no ion flux[46], we have no direct evidence to suggest that such alternative kinetic pathway is indeed populated under physiological conditions. Rather, the present set of hybrid structures might represent the unforeseen consequence of a relatively shallow energy landscape in the context of a non-physiological crystalline lattice (Supplementary material Figure S9).

We suggest that the present structural classes, even if structurally mixed, constitute uniquely valuable assets that provide the basis for a rational molecular mechanism of C-type inactivation in KcsA and by extension, most K^+ channels. In this mechanism, we consider two key conformations for the C-type inactivated filter, I_1 and I_2, each with a distinct backbone structure and ion occupancy profile. I_1 is characterized by a subtle rearrangement in the backbone of Gly77 so that S2 is destabilized and no longer coordinates ions, but S1, S3 and S4 remain viable binding sites. In the I_2 conformation, structural changes in Gly77 are complete, pinching the permeation pathway and fully destabilizing S3, leaving S1 and S4 as the only coordination sites and abrogating ion conduction.

Figure 5b illustrates how this mechanism can account for the experimentally determined electron density profiles corresponding to the individual structural classes. Starting with the

conductive conformation of the filter (O), we consider the two populations of coordinated ions, at S1 and S3 or S2 and S4[23], rendering the familiar four peak electron density profile (Fig 5b). Transitions between stages assume concerted motions among the filter backbone, ions, and water, and are shown as a mixed population of at most two structurally distinct filters to account for the partial peaks observed in the experimental electron densities. In the first transition, because I_1 affects only S2 but not S3, a mixed equilibrium between $O \rightarrow I_1$ shows up as partial reduction in S2. Subsequent transition to mixed equilibrium between $I_1 \rightarrow I_2$ affects both S2 and S3, converging to the experimentally observed two peak profile when most of the channels are in I_2. This corresponds to the key transition, between the Open 17 Å and Open 23 Å classes.

The present model for C-type inactivation does not apply to the brief non-conductive sojourns that characterize flicker channel behaviour, since the present structures represent entry into very stable conformations and not the transient fast closures (10^{-4}–10^{-5} s dwell times) seen in all K^+ channels[47]. Our results and model also argue, rather convincingly, against the rigid nature of the selectivity filter[1,48], suggesting that these multiple structural transitions in the filter can originate from the allosteric coupling between the different regions of the K^+ channel, as described in the accompanying paper[35].

Methods Summary

The constitutively open KcsA mutant tKcsA-OM Δ1-20[38] was expressed in *E. coli* and purified in 10 mM Dodecyl Maltoside, complexed with equimolar amounts of an antibody Fab fragment and crystal trials set up by the sitting drop method in 20–25 % PEG400 (v/v), 50 mM magnesium acetate, 50 mM sodium acetate (pH 5.4–5.6) at 20 °C. The structures were determined by molecular replacement using the Fab fragment and the extracellular part of WT KcsA (PDB 1K4C) without the selectivity filter as search model. Single channel and macroscopic current measurements were carried out by liposome patch clamping as described[49].

Methods

Mutagenesis and expression

For generating tKcsA-OM construct, point mutations were introduced in the KcsA *wild type* DNA sequence by Quikchange protocol, Stratagene La Jolla, California. Truncated KcsA without the first 20 amino acids (tKcsA Δ1-20) was used to generate the constitutively open mutant (KcsA-OM) through the following mutations: H25Q, R117Q, E120Q, R121Q, R122Q and H124Q[32], and was expressed and purified as described[50,51] with slight modifications. In brief, purification was carried out by extracting *E. coli* membranes expressing KcsA with 10 mM DodecylMaltoside (ANATRACE) in a buffer with 150 mM KCl and 50 mM Tris-Cl pH 7.0. Solubilization mixture is spun down @ 100,000 g and the supernatant loaded on to a cobalt column (TALON) and washed extensively with 15 mM imidazole followed by elution with 500 mM imidazole. After purification, protein was loaded on to a Superdex HR 200 (Amersham) size exclusion chromatography to assess proper folding and stability of KcsA.

Liposome patch clamp

Liposome-reconstituted *KcsA* was patch clamped following the method of Delcour et al[49], with some modifications. *KcsA* was reconstituted as above at protein-to-lipid ratios varying from 1:1000 to 1:10000. The proteoliposome suspension was centrifuged for 1 h at 100.000g and the pellet, corresponding to 10 mg of lipids was resuspended in 60 ml of rehydration buffer. Typically, few drops of the suspension were dried overnight in a desiccation chamber

under vacuum for about 24 hours, after which 20 μl of rehydration buffer were applied to each dried drop. Rehydration was allowed for 5 hours, yielding liposomes suitable for patch-clamp. All patch clamp measurements were done at room temperature. Single channel currents were recorded with a Dagan 3900 patch clamp amplifier, currents were sampled at 40 kHz with analog filter set to 5 kHz (−3 dB). Pipette resistances were 5 to 10 MΩ.

Crystallization of KcsA-OM

KcsA open mutant was expressed and purified to homogeneity as described above. KcsA open mutant was crystallized in the presence of antibody Fab fragment by sitting drop method as described previously[34]. Cubic shaped crystal of KcsA-Fab complex appeared after a week in a sitting drop with the following composition 20–25 % PEG400 (v/v), 50 mM magnesium acetate, 50 mM sodium acetate (pH 5.4–5.6) at 20 °C. Based on our previous experience, PEG concentration in the reservoir was increased regularly to decrease the water content in the drop to achieve reduced B-factors. Crystals diffracted to Bragg spacing of 2.6–3.2 Å for all the structures shown. Data was collected on beamlines 23ID (GMCA) and 24IDC (NECAT) at the Advanced Photon Source and processed with HKL2000[52].

Crystallographic analysis

Structures were solved by molecular replacement using only the Fab fragment and the extracellular part of WT KcsA (PDB 1K4C) without the selectivity filter as search model to reduce the biasing of model prediction, as the expected conformation is supposed to be different from the closed state. In the first cycle of refinement using CNS[53], electron density corresponding to the intracellular part with TM2 splayed open appeared, which was filled by manual rebuilding using the program O[54]. Selectivity filter was built with side-chain density corresponding to V76, Y78 and D80 as markers. Multiple cycles of manual rebuilding and refinement was carried out till the complete model is built into the electron density and the R-factors are lowered. Electron density could be seen only up to residue 112-118 in all the structures, and unresolved side-chains were assigned as alanines. Data collection and refinement statistics are given in Supplementary material, Table 1. One-dimensional electron density profiles along the symmetry axis of the selectivity filter for structures were obtained as described elsewhere[23].

Supplementary Material

Refer to Web version on PubMed Central for supplementary material.

Acknowledgments

We thank Drs. F. Bezanilla, B. Roux, H. Mchaourab and R. Nakamoto for helpful discussions and comments on the manuscript. Dr. K. Locher for comments on the manuscripts. Dr. R Mackinnon kindly provided the Fab-expressing hybridoma cells. Drs. S. Chakrapani, J. Cordero-Morales, J. Santos, S. Uysal, O. Dalmas and the members of the Perozo lab for discussions and comments on the manuscript. We are thankful to Dr. Kanagalaghatta R. Rajashankar, Dr. Ruslan Sanishvili and the staff at the NE-CAT 24ID and GM-CA 23ID beamlines at the Advanced Photon Source, Argonne National Laboratory. This work was supported in part by NIH grant R01-GM57846 and by a gift from the Palmer family.

References

1. Doyle DA, et al. The structure of the potassium channel: molecular basis of K^+ conduction and selectivity. Science 1998;280:69–77. [PubMed: 9525859]
2. Kuo A, et al. Crystal structure of the potassium channel KirBac1.1 in the closed state. Science 2003;300:1922–1926. [PubMed: 12738871]

3. Jiang Y, et al. The open pore conformation of potassium channels. Nature 2002;417:523–526. [PubMed: 12037560]
4. Long SB, Campbell EB, Mackinnon R. Crystal structure of a mammalian voltage-dependent Shaker family K+ channel. Science 2005;309:897–903. [PubMed: 16002581]
5. Alam A, Jiang Y. High-resolution structure of the open NaK channel. Nat Struct Mol Biol 2009;16:30–34. [PubMed: 19098917]
6. Jiang Y, et al. X-ray structure of a voltage-dependent K+ channel. Nature 2003;423:33–41. [PubMed: 12721618]
7. Ader C, et al. Structural rearrangements of membrane proteins probed by water-edited solid-state NMR spectroscopy. J Am Chem Soc 2009;131:170–176. [PubMed: 19063626]
8. Baker KA, Tzitzilonis C, Kwiatkowski W, Choe S, Riek R. Conformational dynamics of the KcsA potassium channel governs gating properties. Nat Struct Mol Biol 2007;14:1089–1095. [PubMed: 17922011]
9. Liu YS, Sompornpisut P, Perozo E. Structure of the KcsA channel intracellular gate in the open state. Nature Structural Biology 2001;8:883–887.
10. Perozo E, Cortes DM, Cuello LG. Structural rearrangements underlying K+-channel activation gating [see comments]. Science 1999;285:73–78. [PubMed: 10390363]
11. Takeuchi K, Takahashi H, Kawano S, Shimada I. Identification and characterization of the slowly exchanging pH-dependent conformational rearrangement in KcsA. J Biol Chem 2007;282:15179–15186. [PubMed: 17360718]
12. Loots E, Isacoff EY. Protein rearrangements underlying slow inactivation of the Shaker K+ channel. J Gen Physiol 1998;112:377–389. [PubMed: 9758858]
13. Olcese R, Latorre R, Toro L, Bezanilla F, Stefani E. Correlation between charge movement and ionic current during slow inactivation in Shaker K+ channels. J Gen Physiol 1997;110:579–589. [PubMed: 9348329]
14. Hoshi T, Zagotta WN, Aldrich RW. Biophysical and molecular mechanisms of Shaker potassium channel inactivation. Science 1990;250:533–538. [PubMed: 2122519]
15. Choi KL, Aldrich RW, Yellen G. Tetraethylammonium blockade distinguishes two inactivation mechanisms in voltage-activated K+ channels. Proc Natl Acad Sci U S A 1991;88:5092–5095. [PubMed: 2052588]
16. Hoshi T, Zagotta WN, Aldrich RW. Two types of inactivation in Shaker K+ channels: effects of alterations in the carboxy-terminal region. Neuron 1991;7:547–556. [PubMed: 1931050]
17. Kiss L, Korn SJ. Modulation of C-type inactivation by K+ at the potassium channel selectivity filter. Biophys J 1998;74:1840–1849. [PubMed: 9545046]
18. Kiss L, LoTurco J, Korn SJ. Contribution of the selectivity filter to inactivation in potassium channels. Biophys J 1999;76:253–263. [PubMed: 9876139]
19. Levy DI, Deutsch C. Recovery from C-type inactivation is modulated by extracellular potassium. Biophys J 1996;70:798–805. [PubMed: 8789096]
20. Molina A, Castellano AG, Lopez-Barneo J. Pore mutations in Shaker K+ channels distinguish between the sites of tetraethylammonium blockade and C-type inactivation. J Physiol 1997;499 (Pt 2):361–367. [PubMed: 9080366]
21. Ogielska EM, Aldrich RW. Functional consequences of a decreased potassium affinity in a potassium channel pore. Ion interactions and C-type inactivation. J Gen Physiol 1999;113:347–358. [PubMed: 9925829]
22. Aqvist J, Luzhkov V. Ion permeation mechanism of the potassium channel. Nature 2000;404:881–884. [PubMed: 10786795]
23. Morais-Cabral JH, Zhou Y, MacKinnon R. Energetic optimization of ion conduction rate by the K + selectivity filter. Nature 2001;414:37–42. [PubMed: 11689935]
24. Berneche S, Roux B. Energetics of ion conduction through the K+ channel. Nature 2001;414:73–77. [PubMed: 11689945]
25. Cordero-Morales JF, et al. Molecular determinants of gating at the potassium-channel selectivity filter. Nat Struct Mol Biol 2006;13:311–318. [PubMed: 16532009]

26. Liu Y, Jurman ME, Yellen G. Dynamic rearrangement of the outer mouth of a K+ channel during gating. Neuron 1996;16:859–867. [PubMed: 8608004]
27. Lopez-Barneo J, Hoshi T, Heinemann SH, Aldrich RW. Effects of external cations and mutations in the pore region on C-type inactivation of Shaker potassium channels. Receptors Channels 1993;1:61–71. [PubMed: 8081712]
28. Starkus JG, Kuschel L, Rayner MD, Heinemann SH. Ion conduction through C-type inactivated Shaker channels. J Gen Physiol 1997;110:539–550. [PubMed: 9348326]
29. Alagem N, Yesylevskyy S, Reuveny E. The pore helix is involved in stabilizing the open state of inwardly rectifying K+ channels. Biophys J 2003;85:300–312. [PubMed: 12829485]
30. Lu T, et al. Probing ion permeation and gating in a K+ channel with backbone mutations in the selectivity filter. Nat Neurosci 2001;4:239–246. [PubMed: 11224539]
31. Proks P, Capener CE, Jones P, Ashcroft FM. Mutations within the P-loop of Kir6.2 modulate the intraburst kinetics of the ATP-sensitive potassium channel. J Gen Physiol 2001;118:341–353. [PubMed: 11585848]
32. Cuello LG, et al. Design and characterization of a constitutively open KcsA. FEBS Lett. 2010 In press.
33. Zhou Y, MacKinnon R. The occupancy of ions in the K+ selectivity filter: charge balance and coupling of ion binding to a protein conformational change underlie high conduction rates. J Mol Biol 2003;333:965–975. [PubMed: 14583193]
34. Zhou Y, Morais-Cabral JH, Kaufman A, MacKinnon R. Chemistry of ion coordination and hydration revealed by a K+ channel-Fab complex at 2.0 A resolution. Nature 2001;414:43–48. [PubMed: 11689936]
35. Cuello LG, et al. Structural basis for the coupling between activation and inactivation gates in K^+ channels. Accompanying manuscript. 2010
36. Cuello LG, Cortes DM, Jogini V, Sompornpisut A, Perozo E. A Molecular Mechanism for Proton-Dependent Gating in KcsA. FEBS Lett. 2010 In Press.
37. Thompson AN, Posson DJ, Parsa PV, Nimigean CM. Molecular mechanism of pH sensing in KcsA potassium channels. Proc Natl Acad Sci U S A 2008;105:6900–6905. [PubMed: 18443286]
38. Panyi G, Deutsch C. Cross talk between activation and slow inactivation gates of Shaker potassium channels. J Gen Physiol 2006;128:547–559. [PubMed: 17043151]
39. Domene C, Klein ML, Branduardi D, Gervasio FL, Parrinello M. Conformational changes and gating at the selectivity filter of potassium channels. J Am Chem Soc 2008;130:9474–9480.10.1021/ja801792g [PubMed: 18588293]
40. Kurata HT, Fedida D. A structural interpretation of voltage-gated potassium channel inactivation. Prog Biophys Mol Biol 2006;92:185–208. [PubMed: 16316679]
41. Yellen G. The voltage-gated potassium channels and their relatives. Nature 2002;419:35–42. [PubMed: 12214225]
42. Yellen G, Sodickson D, Chen TY, Jurman ME. An engineered cysteine in the external mouth of a K+ channel allows inactivation to be modulated by metal binding. Biophys J 1994;66:1068–1075. [PubMed: 8038379]
43. Schlief T, Schonherr R, Heinemann SH. Modification of C-type inactivating Shaker potassium channels by chloramine-T. Pflugers Arch 1996;431:483–493. [PubMed: 8596690]
44. Cordero-Morales JF, et al. Molecular driving forces determining potassium channel slow inactivation. Nat Struct Mol Biol 2007;14:1062–1069. [PubMed: 17922012]
45. Noskov SY, Berneche S, Roux B. Control of ion selectivity in potassium channels by electrostatic and dynamic properties of carbonyl ligands. Nature 2004;431:830–834. [PubMed: 15483608]
46. Chakrapani S, Cordero-Morales JF, Perozo E. A quantitative description of KcsA gating I: macroscopic currents. J Gen Physiol 2007;130:465–478. [PubMed: 17938230]
47. Piskorowski RA, Aldrich RW. Relationship between pore occupancy and gating in BK potassium channels. J Gen Physiol 2006;127:557–576. [PubMed: 16636204]
48. Bezanilla F, Armstrong CM. Negative conductance caused by entry of sodium and cesium ions into the potassium channels of squid axons. J Gen Physiol 1972;60:588–608. [PubMed: 4644327]

49. Delcour AH, Martinac B, Adler J, Kung C. Modified reconstitution method used in patch-clamp studies of Escherichia coli ion channels. Biophys J 1989;56:631–636. [PubMed: 2477074]
50. Perozo E, Cortes DM, Cuello LG. Three-dimensional architecture and gating mechanism of a K+ channel studied by EPR spectroscopy. Nat Struct Biol 1998;5:459–469. [PubMed: 9628484]
51. Cortes DM, Perozo E. Structural dynamics of the Streptomyces lividans K+ channel (SKC1): oligomeric stoichiometry and stability. Biochemistry 1997;36:10343–10352. [PubMed: 9254634]
52. Otwinowski Z, Minor W. Processing of X-ray diffraction data collected in oscillation mode. Methods in enzymology 1997;276:307–326.
53. Brunger AT, et al. Crystallography & NMR system: A new software suite for macromolecular structure determination. Acta Crystallogr D Biol Crystallogr 1998;54:905–921. [PubMed: 9757107]
54. Jones TA, Zou JY, Cowans SW, Kjeldgaard M. Improved methods for building protein models in electron-density maps and the location of errors in these models. Acta Crystallog sect 1991;47:110–119.

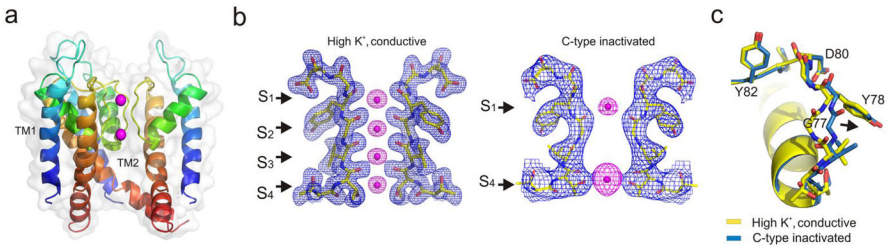

Figure 1.

Crystal structure of Open-Inactivated tKcsA-OM Δ1-20. **a.** Open state of KcsA with one subunit removed for clarity and oriented with the extracellular surface on top. Individual subunits are rainbow coloured from the N-to the C-terminus. **b**. Left, experimental electron density of the closed state (PDB 1k4c) selectivity filter [34]. Shown is the $2F_o-F_c$ electron density map (blue mesh contoured at 2σ) of the filter corresponding to residues 74–80 from two diagonally symmetric subunits. And F_o-F_c omit map (magenta mesh contoured at 6σ) corresponding to ions in the filter. Right, electron density of the open state selectivity filter represented as a composite omit map (blue mesh contoured at 2.0σ) and F_o-F_c omit map (magenta mesh contoured at 6σ) of ions. The polypeptide chain is in stick representation. Ions are represented as spheres. **c**. Comparing the conductive and C-type inactivated selectivity filter structures. The filter conformation in the open state solved in high K^+ is shown in stick representation (Blue, with Oxygen atoms in red). For comparison, the conductive filter in the closed state solved in high K^+ concentration (PDB 1k4c) is shown in yellow. The filter backbone heavy atom rmsd is 1.33 Å with respect to the closed state. All molecular graphics are rendered using Pymol [http://pymol.sourceforge.net].

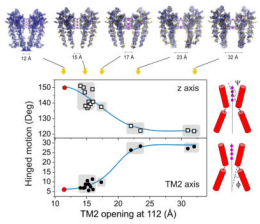

Figure 2.

Conformational classes in Open KcsA structures. Classification of the different open KcsA structures was carried out from geometrical analysis of 15 refined open or partially open structures and the closed structure of KcsA (1K4C). The degree of hinge opening was evaluated from the angle (Ψ) between the z axis (defined by the permeant ions) and the core axis of the C-terminal half of TM2 or the angle (φ) between the N- and C-terminal halves of TM2. Including the fully closed state, we defined five structural classes for the different open and partially open structures of tKcsA-OM Δ1-20, as shown represented by their electron density maps on the top panels. These are the composite omit maps (blue mesh contoured at 2σ) of the channel corresponding to two diagonally symmetric subunits (1K4C-closed state is shown using *2Fo−Fc* electron density map). And $F_o - F_c$ omit map (magenta mesh contoured at 4–6σ) corresponding to ions in the filter. Structural classes are named after the inter-subunit Cα-Cα distances at position T112: Closed (12 Å), plus 15, 17, 23 and 32 Å openings.

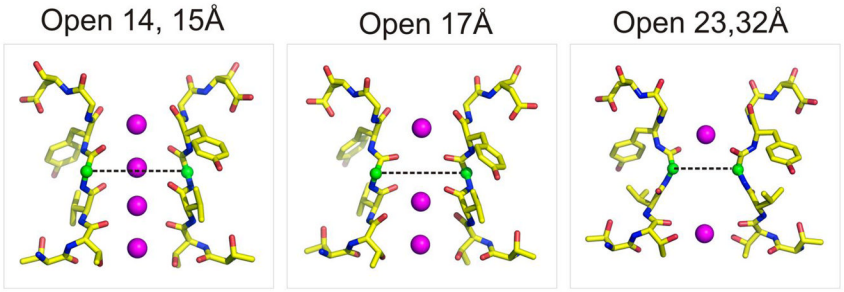

Figure 3.

Correlation between inner gate opening and the conformation of the selectivity filter. Each major structural class is shown as a stick representation with the G77diagonal Cα-Cα distances highlighted by a dotted line. Gate openings associated with the closed, Open 14 and Open 15 Å classes show equivalent filter conformations. After the large transition between the Open 17 and Open 23 Å classes, no major rearrangements of the selectivity filter are observed.

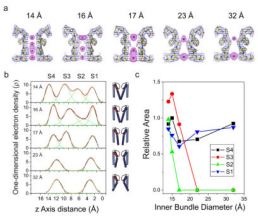

Figure 4.

Correlation between inner gate opening and selectivity filter ion occupancy. **a**. Electron density maps for the different K^+ ion occupancies at the selectivity filter and various degrees of inner bundle gate opening (measured as Cα-Cα distances at T112, top numbers). Shown, in each case, are the composite omit maps (blue mesh contoured at 2σ) of the filter corresponding to residues 74–80 from two diagonally symmetric subunits and the F_o–F_c omit map (magenta mesh contoured at 4–6σ) corresponding to ions in the filter. **b**. Individual one-dimensional electron density profiles along the axis of symmetry (*Z*-axis) for each of the distinct occupancy models, shown using Gly79-Cα as *Z*=0. S1, S2, S3 and S4 represent the binding sites of K^+ ions in the selectivity filter. The cartoon channels represent the relative degree of opening in the inner bundle gate for each density profile. **c**. The dependence of the relative ion occupancies for each of the four K^+ binding sites (S1–S4) with the degree of opening in the inner bundle gate.

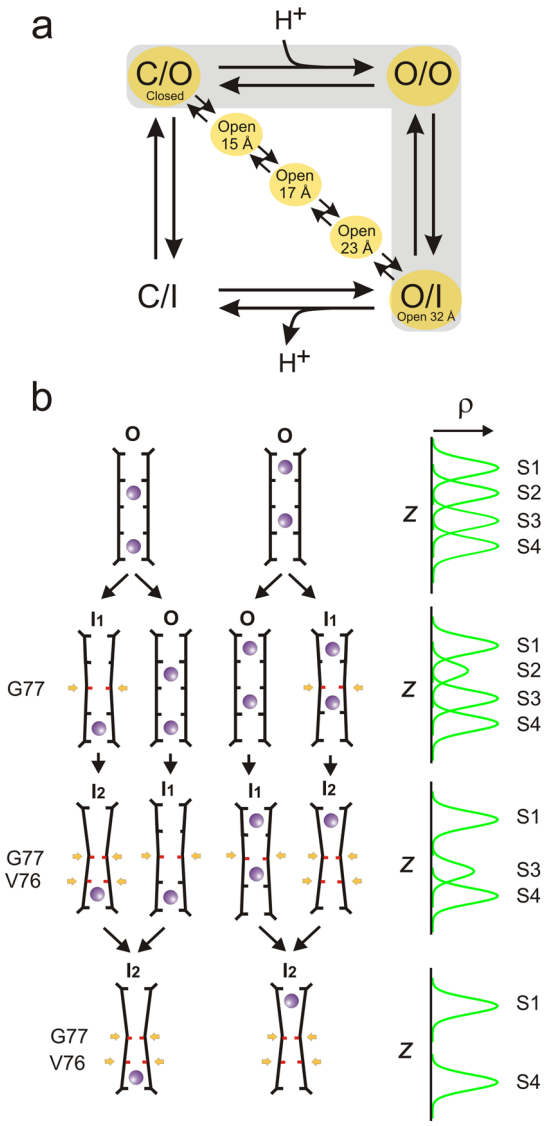

Figure 5.

Structure-based mechanism for C-type inactivation. **a**. The minimal K^+ channel gating cycle highlighting the main kinetic pathway between the closed and open inactivated states (gray background) and the possibility that the hybrid partially open inactivated structures might represent an alternative kinetic pathway. **b**. A mechanistic model of C-type inactivation at the selectivity filter. On the left, the structural transition of selectivity filters of different structures and associated ion occupancies. The selectivity filter evolves form a conductive form of the filter (O) with two ions distributed over four sites (S1–S3, S2–S4) towards an inactivated form of the filter with ion in S1 and S4 (state I_2). This mechanism involves the sequential narrowing of the permeation pathway by pinching at G77 (states I_1 and I_2) and an expected carbonyl reorientation at V76 (state I_2), highlighted in red and sequentially identified by a yellow arrow. In state I_1, the stability of S2 is compromised (but not that of S1, S3 and S4), while state I_2 is associated with a loss of S3. In each stage, a mixed population is depicted as a way to account for the experimental one-dimensional electron density map, shown in idealized form on the right.